Photonic Network Analyzer Based on Optical Sampling

Min Ding, Zhengtao Jin, Jianping Chen, and Guiling Wu

***Abstract*— A wideband photonic network analyzer (PNA) for microwave devices based on optical sampling is reported. Optical sampling is implemented to capture the response signals from devices under test for scattering parameter, sparing intricate procedures of down conversion in traditional electrical network analyzers. To validate the theoretical analysis, we establish an experimental PNA with a measurable frequency span up to 35 GHz, which can reach 100 GHz by applying a faster commercial modulator. Moreover, the scattering parameter magnitude of a 25 GHz low pass filter is measured by the established PNA. The experimental result is well consistent with that of a commercial network analyzer.**

***Index Terms*— Microwave photonics, network analysis, optical sampling, scattering parameter mesurement.**

I. Introduction

THE network analyzer is at the heart of the research and development of plentiful electrical components and systems [1]. The ever increasing demand on high frequency in various fields like radar, communication, and semiconductor is driving network analyzers to advance towards larger measurable frequency span. Two typical receiver architectures, heterodyne and homodyne, have been proposed for electrical network analyzers (ENAs) to down-convert the response signals from devices under test (DUTs) to the intermediate frequency signals. The superior sensitivity and selectivity of heterodyne receivers are at the cost of volume and power dispassion increases with the sever trade-off between image rejection and channel selection and between gain and noise figure [2]. Homodyne receivers are relatively simple, but also faced with challenges like direct current (DC) offset, local oscillator leakage, and I/Q mismatch [3], [4].

The rapid progress of microwave photonics provides innovative solutions for microwave & radio frequency engineering, including the network analysis. In the previous researches, Frankel, M. Y, et al presented a network analyzer based on the time domain method, recording the impulse response from DUTs. Electrical transient pulses stimulate the DUTs to generate the time domain impulse response which is recorded with equivalent time sampling [5]. Subsequently, the frequency domain characteristic is obtained by applying the Fourier transform on the impulse response. However, the measurement on narrowband DUTs is beyond the ability of this scheme, which introduces the interference between adjacent pulses [6]. Furthermore, the finite modulation efficiency in this scheme leads to a poor signal to noise ratio [7]. Also based on the time domain method, Lonappan et. al. proposed an improvement scheme for the impulse response recording with time stretch technology [8], [9]. In this scheme, the deterioration of the signal-to-noise ratio limits the system dynamic range since signal intensity is attenuated with time stretching [10]. Moreover, some approaches based on the frequency domain method are reported as well. Sascha Preu proposed a THz network analyzer with homodyne detection [11]. Nevertheless, the proposed homodyne network analyzer, applying only one demodulation channel, is incapable of reading out both the amplitude and phase information from the DC term. In the practical application, the homodyne detection still entails essential issues, such as I/Q mismatch [2], [3]. There is also a frequency extension scheme based on traditional ENAs with heterodyne detection presented by Criado et al, remaining the unsolved problem of the low conversion efficiency and the low power value [12].

In this letter, we propose a photonic network analyzer (PNA) employing optical sampling, not only realizing a wideband measurement but also discarding the tedious frequency mixing process in traditional ENAs. The proposed PNA adopts the frequency domain method to acquire the scattering parameter (S parameter) magnitude, where a DUT is under the stimulation of a continuous wave sinusoidal signal with a swept frequency and produces corresponding response signals. After that, an optical sampling pulse train directly captures the response signals, followed by the photodetection and quantization. The S parameter magnitude is calculated from the quantized results with digital signal processing. Since the PNA bandwidth is determined by the temporal shape of the single optical pulse and the frequency response of the modulator, it can reach a bandwidth over 100 GHz with commercial devices. We carry out an experimental PNA and measures the S parameter magnitude of a 25 GHz low pass filter from 1 to 35 GHz. The experimental result of the PNA is shown and compared with that of a commercial ENA.

II. Principle

The PNA on the basis of optical sampling, whose schematic diagram is shown in Fig. 1, comprises four modules: signal generation, test set, receiver, and signal processing. During signal generation, a microwave source (MS) generates a sinusoidal signal within the desired frequency span, which is transmitted to the test set as the incident signal of the DUT. The function of the test set is to separate reflected

Manuscript received December 10, 2019; revised January 3, 2020; accepted January 15, 2020. Date of publication January 21, 2020; date of current version January 29, 2020. This work was supported in part by the National Natural Science Foundation of China (NSFC) under Grant 61535006 and Grant 61627817. *(Corresponding author: Guiling Wu.)*

The authors are with the State Key Laboratory of Advanced Optical Communication Systems and Networks, Department of Electronic Engineering, Shanghai Jiao Tong University, Shanghai 200240, China (e-mail: wuguiling@sjtu.edu.cn).

Color versions of one or more of the figures in this letter are available online at http://ieeexplore.ieee.org.

Digital Object Identifier 10.1109/LPT.2020.2968377

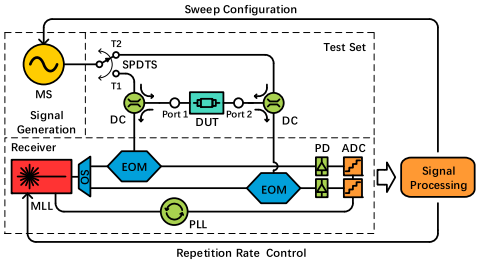

Fig. 1. Schematic diagram of the proposed photonic network analyzer based on analog optical sampling link. MS: Microwave Source; SPDTS: Single-Pole Double-Throw Switch; DC: Directional Coupler; DUT: Device Under Test; MLL: Mode-Locked Laser; OS: Optical Splitter; EOM: Electro-Optic Modulator; PD: Photodetector; ADC: Analog-to-Digital Converter; PLL: Phase-Locked Loop.

signal and transmitted signal, where a single-pole double-throw switch (SPDTS) is applied to select the input port of the DUT, corresponding to the forward and reverse stimulation. The reflected and transmitted signals are extracted respectively by directional couplers (DCs) on both sides of the DUT prior to entering an optical sampling based receiver. In the receiver, a sampling optical pulse train from a mode-locked laser (MLL) is divided into two channels by an optical splitter (OS) to respectively sampling the reflected and transmitted signals via electro-optic modulators (EOMs). After the optical pulses loaded with the response signal are converted into the electrical ones by photodetectors (PDs) in two channels, the reflected and transmitted signals are digitized by analog to digital converters (ADCs). The sampling rate of ADCs is synchronized with the sampling optical pulse train repetition rate with a phase-locked loop (PLL). The signal processing module calculates the relative magnitude of the reflected and transmitted signal to the incident signal respectively to extract the S parameter magnitude at a specified frequency point.

The reflected/transmitted signal from DUT can be expressed as

$$v'_{ij}(t) = v_I(t) * s_{ij}(t), \quad i = 1, 2 \quad j = 1, 2, \tag{1}$$

where $v_I(t)$ is the sinusoidal incident signal from the MS, $s_{ij}(t)$ is the S parameters of the DUT expressed in the time domain, i and j respectively represent the output and the input port of the DUT. The operator $*$ denotes the convolution operation. The temporal power shape of the sampling optical pulse train in the receiver can be expressed as

$$p(t) = P_A \sum_{n=-\infty}^{\infty} p_s(t - nT_s), \tag{2}$$

where P_A is the average power of the optical pulse train, $p_s(t)$ is the temporal power shape of single optical pulse normalized by P_A, and T_s is the period of the sampling optical pulse train. Mach-Zehnder Modulator (MZM) is usually employed as the EOM in each channel. When the MZMs are biased at quadrature and the small signal condition is satisfied, the reflected/transmitted signal is modulated onto the sampling optical pulse train linearly [13], and we have the optical pulse train after the MZMs:

$$p_M(t) = 0.5[1 - h_M(t) * v'_{ij}(t)]p(t), \tag{3}$$

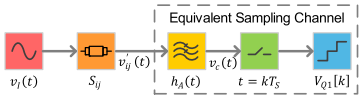

Fig. 2. Equivalent model of the modulated component.

where $h_M(t)$ is the impulse response of the MZMs and other electrical components in the test set including the SPDTS, the DCs, and the cables. In the case where the input optical power is far less than the saturation power, the responsivity of PDs can be regarded as linear. The photodetection with PDs and the quantization with ADCs yield a digitized signal, $v_Q[k]$, composing of an unmodulated component, $v_{Q0}[k]$, and a modulated component, $v_{Q1}[k]$, [14]:

$$\begin{cases} v_Q[k] = v_{Q0}[k] + v_{Q1}[k] \\ v_{Q0}[k] = 0.5p(t) * h_E(t - d_E)|_{t=0} \\ v_{Q1}[k] = h_A(t) * v'_{ij}(t)\Big|_{t=kT_s} \end{cases}, \tag{4}$$

where $h_A(t)$ is an equivalent impulse response expressed as

$$h_A(t) = -0.5[h_E(t - d_E)p(-t)] * h_M(t). \tag{5}$$

In Eq.(5), $h_E(t)$ is the electrical back-end impulse response including the devices from the PDs to the ADCs, and d_E represents a delay from the MZMs to the ADCs. It can be seen from Eq. (4) that the unmodulated component, $v_{Q0}[k]$, is a constant irrelevant to the incident signal, $v'_{ij}(t)$, and the modulated component, $v_{Q1}[k]$, is a sinusoidal wave relevant to $v'_{ij}(t)$. Therefore, $v_{Q0}[k]$ can be removed from $v_Q[k]$ by subtracting the average value of $v_Q[k]$. According to Eq. (4), the modulated component acquisition is equivalent to the stages displayed in Fig. 2. Firstly, the DUT, stimulated by the incident signal $v_I(t)$, produces the response signal $v'_{ij}(t)$ carrying the desired S parameter and then the $v'_{ij}(t)$ is filtered by the equivalent channel impulse response $h_A(t)$. After sampling and quantizing the filtered signal $v_c(t) = h_A(t) * v_I(t) * s_{ij}(t)$, one can acquire the digital modulated component $v_{Q1}[k]$.

From Eq. (5), one can see that the system bandwidth depends on its equivalent channel frequency response, $h_A(t)$. The corresponding equivalent channel frequency response can be derived:

$$H_A(\Omega) = -0.5H_M(\Omega)P_s(\Omega)R(\Omega), \tag{6}$$

where

$$R(\Omega) = \frac{1}{T_s} \sum_{n=-\infty}^{\infty} H_E(\Omega + n\Omega_s)\exp[-j(\Omega + n\Omega_s)d_E]. \tag{7}$$

In Eqs. (6) and (7), the functions denoted by an upper case letter are the Fourier Transform of the functions expressed by the corresponding lower case letter, and $\Omega_s = 2\pi/T_s$. $R(\Omega)$ is a term representing the inter-symbol interference (ISI) which can be introduced by overlap between adjacent electrical pulses in the time domain. When the bandwidth of electrical back-end is over half of the sampling rate, ISI will not be introduced in the system and $R(\Omega)$ remains a constant value. In this case, the equivalent channel frequency response forms a continuous passband and the system bandwidth is no longer limited by the bandwidth of the electrical back-end but determined by the product of the $H_M(\Omega)$ and $P_s(\Omega)$. The state of the art of MZM has reached a bandwidth of several

hundreds of GHz [15], [16]. The temporal width of mature pulse lasers has been able to reach femtosecond [17], [18]. For a 3 ps Gaussian pulse, its bandwidth is already approximated to 100 GHz. Therefore, the PNA has a potential for a wide measurable frequency span to hundreds of GHz with a relaxed bandwidth requirement of the electrical back-end including PDs and ADCs.

The desired S parameter can be derived from the modulated component of the sampling result. From Eq. (4), the frequency spectrum of the modulated component in the digital domain is

$$V_{Q1}(\Omega) = \sum_{k=-\infty}^{\infty} V_c(\Omega - k\Omega_s)\Big|_{\Omega=\frac{\omega}{T_s}} = \sum_{k=-\infty}^{\infty} V_c(\frac{\omega - 2k\pi}{T_s}), \quad (8)$$

where

$$V_c(\Omega) = V_I(\Omega)S_{ij}(\Omega)H_A(\Omega), \quad (9)$$

In Eqs. (8) and (9), the functions taking Ω and ω as a variable respectively represent the Fourier transform in the analog and digital domain of the corresponding time domain signal.

Since the DUT is modeled as a linear time-invariant system in the network analysis, and the equivalent channel impulse response of the system is also linear, the filtered signal $V_c(\Omega)$ can be considered as a sinusoidal signal with the same frequency as the incident signal $V_I(\Omega)$. From Eq. (8), when the frequency of $V_C(\Omega)$ is within the first Nyquist zone, the optical sampling rate is sufficient to directly represent $V_c(\Omega)$. When the frequency of $V_C(\Omega)$ is beyond the first Nyquist zone, the signal will be undersampled and aliased to the first Nyquist zone with the same magnitude. Since $V_c(\Omega)$ is single-tone, the magnitude of the original signal could be represented by that of the aliased signal in the first Nyquist zone. Therefore, a raw S parameter magnitude within the bandwidth of $H_A(\Omega)$ is obtained by calculating the relative magnitude of $V_C(\Omega)$ to the incident signal $V_I(\Omega)$.

After the raw S parameter magnitude measurement, it is necessary to perform a response calibration to suppress the influence of the equivalent channel impulse response. According to Eq. (4), the calibrated S parameter magnitude can be calculated by

$$|S_{ij}(\Omega)| = |V_c(\Omega)|/|V_I(\Omega)H_A(\Omega)|, \quad (10)$$

where $H_A(\Omega)$ is obtained by connecting Port 1 and Port 2 with calibration standards (a thru for transmitted S parameters, an open or a short for reflected S parameters) [19]. It is worth noting that at frequency points which are multiples of the optical pulse repetition, the sampling result is DC and contains no magnitude information. This circumstance can be avoided by changing the repetition of the optical pulse train through controlling the cavity length of the MLL [20].

III. Experiment

We have experimentally implemented the proposed PNA shown in Fig. 1 to verify the performance of this scheme. A sinusoidal incident signal from an MS (Rohde & Schwarz, SMF 100A) is loaded onto the DUT through the test set where all the devices have a bandwidth beyond 40 GHz. An MLL (Precision Photonics, FFL1560) generates a sampling optical pulse train with a repetition rate of 36.5 MHz at 1560 nm center frequency. In each channel, a 40 Gbps MZM biased at quadrature with a half-wave voltage of 5.4 V modulate the transmitted/reflected signal from the test set onto the sampling optical pulse train. After detected by a PD with a bandwidth of 300 MHz, the optical pulse carrying the response signal is converted into the electrical counterpart. The electrical pulses are quantized by a multichannel digitizer (Keysight, M9703A) synchronized with the repetition rate of the optical sampling pulse train from the MLL. Since the 1.2 GHz bandwidth of the digitizer is much larger than 300 MHz, the electrical back-end bandwidth is mainly determined by the PD, which is more than half of the 36.5 MHz optical sampling rate, satisfying the no ISI condition.

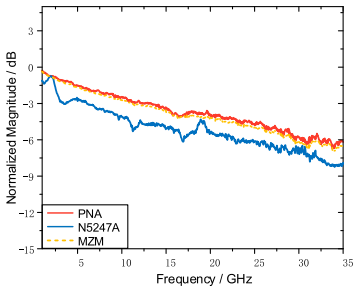

Fig. 3. The system frequency response of the PNA and the commercial ENA.

Figure 3 shows the system frequency response of the adopted MZM, the experimental PNA and the commercial ENA (Keysight, PNA-X N5247A). The attenuation at 35 GHz of PNA and the commercial ENA are $\sim$ −6.18dB and $\sim$ −7.89 dB, respectively. The employed optical pulses have a temporal width of less than 1 ps (corresponding to $\sim$300 GHz bandwidth), which is much wider than that of the MZM. Therefore, the PNA bandwidth in this experiment should be determined by the adopted MZM bandwidth, as Eq. (6) indicates. As shown in Fig. 3, the PNA frequency response is basically identical to that of the MZM, which is consistent with the theoretical analysis. Moreover, by replacing the adopted MZM with a wider bandwidth MZM, we can extend the PNA bandwidth further.

To test the PNA performance, we measure a 25 GHz low pass filter from 1 to 35 GHz with 2001 sweeping points. The corresponding frequency resolution is 17 MHz, which can be improved by increasing the sweeping points. The highest frequency resolution of the proposed PNA is determined by the adopted MS. The incident signal power is set to 0 dBm to ensure the system linearity, corresponding to a modulation index of $\sim$0.18. The S parameter magnitude of the filter measured by the PNA is compared with that of the commercial ENA. The calibrated S parameter magnitude, $|S_{11}|$, $|S_{12}|$, $|S_{21}|$, and $|S_{22}|$, is shown in Fig. 4. The DUT insertion loss is $\sim$0.01 dB at 1 GHz and the return loss is $\sim$0.7 dB at 35 GHz. From $|S_{12}|$ and $|S_{21}|$ measurement, one can see that the dynamic range of the PNA can reach up to 60 dB. The deviation of the $|S_{12}|$ and $|S_{21}|$ between PNA and N5247A curves within 28 GHz is less than 1 dB and after $\sim$28 GHz both curves are buried in noises for the

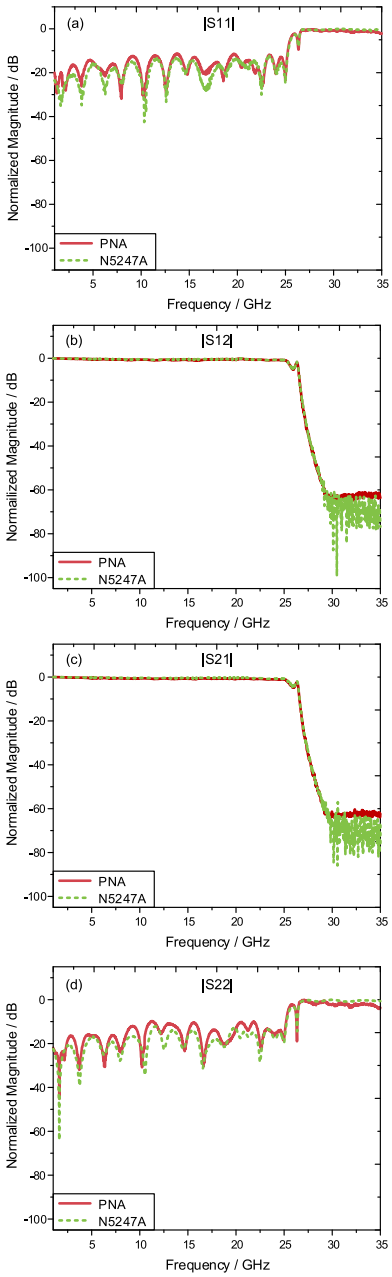

Fig. 4. Measured magnitudes of S parameter of a 25 GHz low pass filter. (a) $|S_{11}|$, (b) $|S_{12}|$, (c) $|S_{21}|$ and (d) $|S_{22}|$.

limitation of dynamic range. The main noise sources in the PNA include the amplitude fluctuation and timing jitter of the optical sampling pulse trains, aperture jitter noise of the synchronizing circuits, quantization noise of the ADCs and noise of the PDs (thermal noise, shot noise, etc.). The MLL provides ultrahigh stable optical sampling pulse train, which implies that the amplitude fluctuation and timing jitter are not dominant. The aperture jitter noise can be suppressed by sampling electrical pulses at their peaks. Compared with the noise from PDs, the quantization noise of high-resolution ADCs can be neglected. Therefore, the measurement results in the PNA is mainly polluted by the noise of the PDs. The directivity and crosstalk error from the electrical directional couplers, and the mismatches of sources and loads are two of the potential causes resulting in the deviation of the $|S_{11}|$ and $|S_{22}|$ between PNA and N5247A measurement.

IV. Conclusion

In conclusion, a novel photonic network analyzer is presented for the S parameter magnitude measurement of microwave devices in this letter. The proposed PNA features the optical sampling based receiver which enables a wide measurable frequency span, obviating the need for the complicated down-conversion in common ENAs. The PNA principle and system bandwidth are analyzed theoretically and verified experimentally up to 35 GHz. The experimental result is basically agree with that of a commercial ENA. With further improvement of the system structure and the signal processing algorithm, the proposed PNA has the potential to extend the phase measurement function.

References

[1] D. Rytting, "ARFTG 50 year network analyzer history," in *Proc. 71st ARFTG Microw. Meas. Conf.*, Jun. 2008.
[2] S. Mirabbasi and K. Martin, "Classical and modern receiver architectures," *IEEE Commun. Mag.*, vol. 38, no. 11, pp. 132–139, Nov. 2000.
[3] B. Razavi, "Design considerations for direct-conversion receivers," *IEEE Trans. Circuits Syst. II. Analog Digit. Signal Process.*, vol. 44, no. 6, pp. 428–435, Jun. 1997.
[4] M. Inamori, A. Bostamam, Y. Sanada, and H. Minami, "IQ imbalance compensation scheme in the presence of frequency offset and dynamic DC offset for a direct conversion receiver," *IEEE Trans. Wireless Commun.*, vol. 8, no. 5, pp. 2214–2220, May 2009.
[5] M. Frankel, J. Whitaker, G. Mourou, and J. Valdmanis, "Ultrahigh-bandwidth vector network analyzer based on external electro-optic sampling," *Solid-State Electron.*, vol. 35, no. 3, pp. 325–332, Mar. 1992.
[6] M. Frankel, J. Whitaker, and G. Mourou, "Optoelectronic transient characterization of ultrafast devices," *IEEE J. Quantum Electron.*, vol. 28, no. 10, pp. 2313–2324, Oct. 1992.
[7] J. Valdmanis and G. Mourou, "Subpicosecond electrooptic sampling: Principles and applications," *IEEE J. Quantum Electron.*, vol. JQE-22, no. 1, pp. 69–78, Jan. 1986.
[8] C. K. Lonappan, A. M. Madni, and B. Jalali, "Single-shot network analyzer for extremely fast measurements," *Appl. Opt.*, vol. 55, no. 30, p. 8406, Oct. 2016.
[9] Z. Bai, C. K. Lonappan, T. Jiang, A. M. Madni, F. Yan, and B. Jalali, "Tera-sample-per-second single-shot device analyzer," *Opt. Express*, vol. 27, no. 16, p. 23321, Aug. 2019.
[10] F. Coppinger, A. Bhushan, and B. Jalali, "Photonic time stretch and its application to analog-to-digital conversion," *IEEE Trans. Microw. Theory Techn.*, vol. 47, no. 7, pp. 1309–1314, Jul. 1999.
[11] S. Preu, "Components towards a photonics aided THz vector network analyzer," in *Proc. Opt. Fiber Commun. Conf.*, Mar. 2016, pp. 1–3.
[12] A. R. Criado, C. de Dios, P. Acedo, and H. L. Hartnagel, "New concepts for a photonic vector network analyzer based on THz heterodyne phase-coherent techniques," in *Proc. Microw. Integr. Circuits Conf. (EuMIC), 7th Eur.*, Oct. 2012, pp. 540–543.
[13] J. Mckinney and K. Williams, "Sampled analog optical links," *IEEE Trans. Microw. Theory Techn.*, vol. 57, no. 8, pp. 2093–2099, Aug. 2009.
[14] F. Su, G. Wu, L. Ye, R. Liu, X. Xue, and J. Chen, "Effects of the photonic sampling pulse width and the photodetection bandwidth on the channel response of photonic ADCs," *Opt. Express*, vol. 24, no. 2, p. 924, Jan. 2016.
[15] K. Noguchi, O. Mitomi, and H. Miyazawa, "Millimeter-wave Ti:$LiNbO_3$ optical modulators," *J. Lightw. Technol.*, vol. 16, no. 4, pp. 615–619, Apr. 1998.
[16] C. Hoessbacher *et al.*, "Plasmonic modulator with >170 GHz bandwidth demonstrated at 100 GBd NRZ," *Opt. Express*, vol. 25, no. 3, p. 1762, Feb. 2017.
[17] K. Kieu and M. Mansuripur, "Femtosecond laser pulse generation with a fiber taper embedded in carbon nanotube/polymer composite," *Opt. Lett.*, vol. 32, no. 15, p. 2242, Aug. 2007.
[18] T. R. Schibli *et al.*, "Ultrashort pulse-generation by saturable absorber mirrors based on polymer-embedded carbon nanotubes," *Opt. Express*, vol. 13, no. 20, p. 8025, Nov. 2005.
[19] D. Ballo, "Applying error correction to network analyzer measurements," *Microw. J.*, vol. 41, no. 3, pp. 64–81, 1998.
[20] D. Hou, J. Wu, Q. Ren, and J. Zhao, "Analysis of long-term phase-locking technique for mode-locked laser with PID regulator," *IEEE J. Quantum Electron.*, vol. 48, no. 7, pp. 839–846, Jul. 2012.